Chalcogenide Letters Vol. 22, No. 8, August 2025, p. 707 - 717

# Synthesis, characterization of zirconium doped cobalt nanoparticles and study of their thermoelectric properties

Y. Arooj [a], A. Farhan [b], S. Maqsood [a,c], A. Erum [a], M.Ishaq [d], S. Rafique [a], A. Khalid [b], F. Wazahat [a], M. A. Qamar [e,*]

[a] *Department of Physics, Government College Women University Faisalabad, Faisalabad 38000, Pakistan*

[b] *Department of Chemistry, University of Agriculture Faisalabad, Faisalabad, Pakistan*

[c] *Department of Physics, University of Agriculture Faisalabad, Faisalabad, Pakistan*

[d] *Department of Physics, Riphah International University Faisalabad Campus, Faisalabad.*

[e] *Department of Chemistry, School of Science, University of Management and Technology, Lahore 54770, Pakistan*

Chemical co-precipitation synthesis was used to make pure and zirconium-doped cobalt sulfide ($Co_3S_4$) nanoparticles (NPs). Important characterizations such as FTIR, UV-VIS, Raman, PL, SEM, XRD, and four probe methods were used to examine the influence of the Zr (0%, 5%, 10%, 15%, and 20%) doping on optical, electrical, structural, and thermoelectric characteristics of $Co_3S_4$ NPs. X-ray diffraction and SEM examination verified the cubic structure and grain size of pure and Zr-doped $Co_3S_4$-NPs. The FTIR spectrum revealed the rotational and vibrational modes linked to the material's surface. The material is optimal for photocatalytic activity with a redshift in the band gap value (Eg) as a function of Zr dopant and exhibit very good absorbance in the optical region. Raman and PL spectroscopy examined the vibrational modes, optical and electrical properties of the prepared samples. The measurement of the thermoelectric effect showed that all samples approached the critical value of the temperature where the current started decreasing.

(Received May 15, 2025; Accepted August 11, 2025)

*Keywords*: Aqueous, Cobalt sulfide, Rotational, Grain size, Elemental composition

## 1. Introduction

To minimize or eliminate the usage of valuable metals, substantial efforts have been devoted to developing and designing an electrocatalyst with higher performance and stability [1]. Different catalysts have been described, such as transition metal oxide [2, 3], sulfide [4], phosphide [5], nitride [6], and selenide [7]. Among these catalysts, transition metal sulfide has shown substantial benefits like cheap cost, low electronegativity, eco-friendly nature, and powerful electrocatalytic performance [8, 9]. In practice, cobalt sulfides have been intensively explored as an excellent candidate for OER catalysts due the strong electrical conductivity and excellent anti-corrosive [10, 11].

Cobalt Sulfide nanoparticles have physical and chemical properties depending on their size. These properties can be examined by using various techniques like hydrothermal technique [12], microwave irradiation technique [13], sol-gel technique [14], electrodeposition technique [15], and co-precipitation technique [16].

The performance of a reaction using a catalyst can be catalyzed, and it increases the efficiency of the whole process. The doping of atoms in the host material and the heterojunction enhances the level of the energy to perform the fastest recombinations or the transfer of the charge [17]. Sulfides have very low electronegativity, and then the atoms having large atomic radii showed

* Corresponding author: qamariub@gmail.com
https://doi.org/10.15251/CL.2025.228.707

large ionic conductivity, making them a suitable choice for applications at the practical level [18-20]. Nanoparticles doped with transition metals have various optical properties related to their host counterparts [21]. This type of nanoparticles is utilized in many applications like solar cells, catalysis and optical light emitting devices i.e., diodes, resonant tunneling devices, lasers, electroluminescent devices, phosphors, light emitting displays, and optical sensors [22, 23].

Zirconium is universally present in abundance and can be obtained by the plants [24], and studies has demonstrated that the doping of Zr inhibits structural and functional group modifications [25, 26, 27]. Zr doping may enhance the specific surface area of substance, therefore increasing more active sites availability. Thus, Zr doping on cobalt sulfide looks promising approach [28, 29]. Therefore, in the current research we targeted the synthesis of Zr doped $Co_3S_4$-NPs and study of their I-V characteristics, and thermoelectric properties.

## 2. Experimental section

Cobalt chloride hexahydrated ($CoCl_2.6H_2O$) as a source for cobalt, Sodium Sulfide flakes ($Na_2S$) serve as S source, Zirconium oxychloride octahydrate ($ZrOCl_2.6H_2O$) as a source of Zr, ($NH_4OH$) used as a capping agent, Ethylene glycol, Distilled water, Ethanol. In terms of purity, all of the compounds were up to standard.

Pure cobalt sulfide was prepared via an aqueous chemical co-precipitation technique [30]. In 100ml distilled water, a 0.1M solution of $CoCl_2.6H_2O$ and $Na_2S$ was used with continuous stirring. Drop by drop, $Na_2S$ solution was added to $CoCl_2$ solution with continuous stirring, resulting in a black-colored cobalt sulfide solution. As a capping agent, ammonia was applied. The resulting solution was agitated at 60°C for 90 minutes. After bringing it to ambient temperature, it was repeatedly cleaned with deionized water/ethanol and then dried at 80°C for 3 hours. At the end, the calcination of black powder was done for 3 hours at 450°C.

Zr-doped cobalt sulfide with different concentration levels was synthesized using a solution of 0.1M of $CoCl_2.6H_2$ with constant stirring in 100ml distilled water. To obtain 5%, 10%, 15%, 20% by volume Zr doping, 5 ml, 10 ml, 15 ml, and 20 ml of $ZrOCl_2.6H_2O$ solution was added to 95 ml, 90 ml, 85 ml, and 80 ml of $CoCl_2$ solution, respectively. The rest of the procedure is the same as for Cobalt Sulfide without doping. Finally, the synthesized samples were calcined for 3 hours at 450°C. Using a mortar and pestle, the finished substances were homogenized. In this study, the undoped and 5%, 10%, 15%, and 20% Zr-doped $Co_3S_4$ samples were used, respectively.

X-ray diffraction (monochromatic Cu (K$\alpha$) $\lambda = 1.54A^o$) was used to determine the structural characteristics (XRD). XRD data was collected in a 20° to 60° diffraction angle step. CNAMR Scanning Electron Microscope (SEM) at 5kV was used to determine the morphology of the sample. The various functional groups linked to the synthesised sample were seen using a Bruker spectrometer and Fourier Transform Infrared Spectroscopy (FTIR). Perkin Elmer UV-Visible Spectrometer was utilized to examine the optical properties of samples. Two probes (IV) technique investigated electrical characteristics (conductivity and resistivity) as well as thermoelectric qualities. Optical and electrical properties were discussed by PL Spectroscopy. Specified vibrational modes of the Cobalt sulfide were mentioned by Raman Spectroscopy.

## 3. Results and discussion

### 3.1. XRD analysis

The X-rays diffraction (XRD) characterization technique has been widely used to determine crystal structure and lattice parameters of the lattice [31]. XRD investigation of zirconium-doped cobalt sulfide gives substantial structural information regarding the effect of zirconium integration on the material's crystalline characteristics. The XRD patterns, acquired over a 2θ range of 20° to 60°, reveal distinct diffraction peaks related to the $Co_3S_4$ phase. Undoped cobalt sulfide and doped cobalt sulfide samples were named as F1, F2, F3, F4, and F5 on the basis of the concentration of doping of Zr (0, 0.1, 0.15, 0.2, 0.25). XRD of synthesized materials has been shown in *Fig. 1*. There

are diffraction peaks with planes (220), (222), and (331) that correspond to diffraction angles of 27.09°, 32.89°, and 36.75°. Using diffraction angles and the indexed plane, a cubic structure with lattice constant at 7.9 $A^o$ is computed, which is in good accord with a previously published study [32]. Furthermore, using the Scherrer equation [33], the average crystallite size of pure and Zr doped $Co_3S_4$-NPs in the 2.29 to 54.42 nm range was determined.

$$D = \frac{K\lambda}{\beta Cos\theta} \quad (1)$$

where $\beta$ indicates full width at half maxima (FWHM) value in radians, θ indicates angle measure in radians and $\lambda$ indicates wavelength of x-rays. The standard value of $\lambda$ is 1.54059.

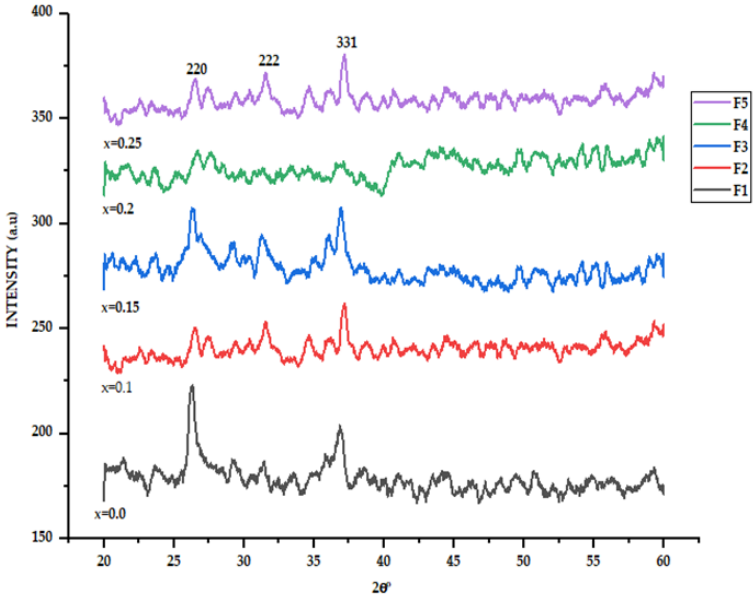


*Fig. 1. XRD pattern of Zr (0, 0.1, 0.15, 0.2, 0.25) doped $Co_3ZrxS_4$*

### 3.2. Surface and elemental analysis (SEM)

SEM is a very effective tool for identifying morphological growth. The morphology and size of particle for five $Co_3S_4$ samples were evaluated and studied using SEM. The results of SEM for pure and doped cobalt sulfide ($Co_3Zr_xS_4$) nanoparticles (x=0, 0.1, 0.15, 0.2, 0.25) are shown in the Figs.2 (a-e). The average grain size of the synthesized nanoparticle is 14 nm. The grain size of the pure sample ($Co_3S_4$) is 22.7 nm (Fig.2a). The small particles in agglomerated shapes were discovered in pure sample that did not have Zr doping. As shown in Figs.2 (b-e), particles with Zr doping were less prone to form agglomerated clusters. Cobalt Sulfide ($Co_3Zr_xS_4$) nanoparticles (0.1, 0.15, 0.2, 0.25) that were doped with Zr showed 9.5nm, 8.1 nm, 17.2 nm, and 9.93 nm, respectively. The size of particle is considered to be the function of the Zr doping. SEM images confirmed the synthesis of pure $Co_3S_4$, and doped Zr-based $Co_3S_4$.

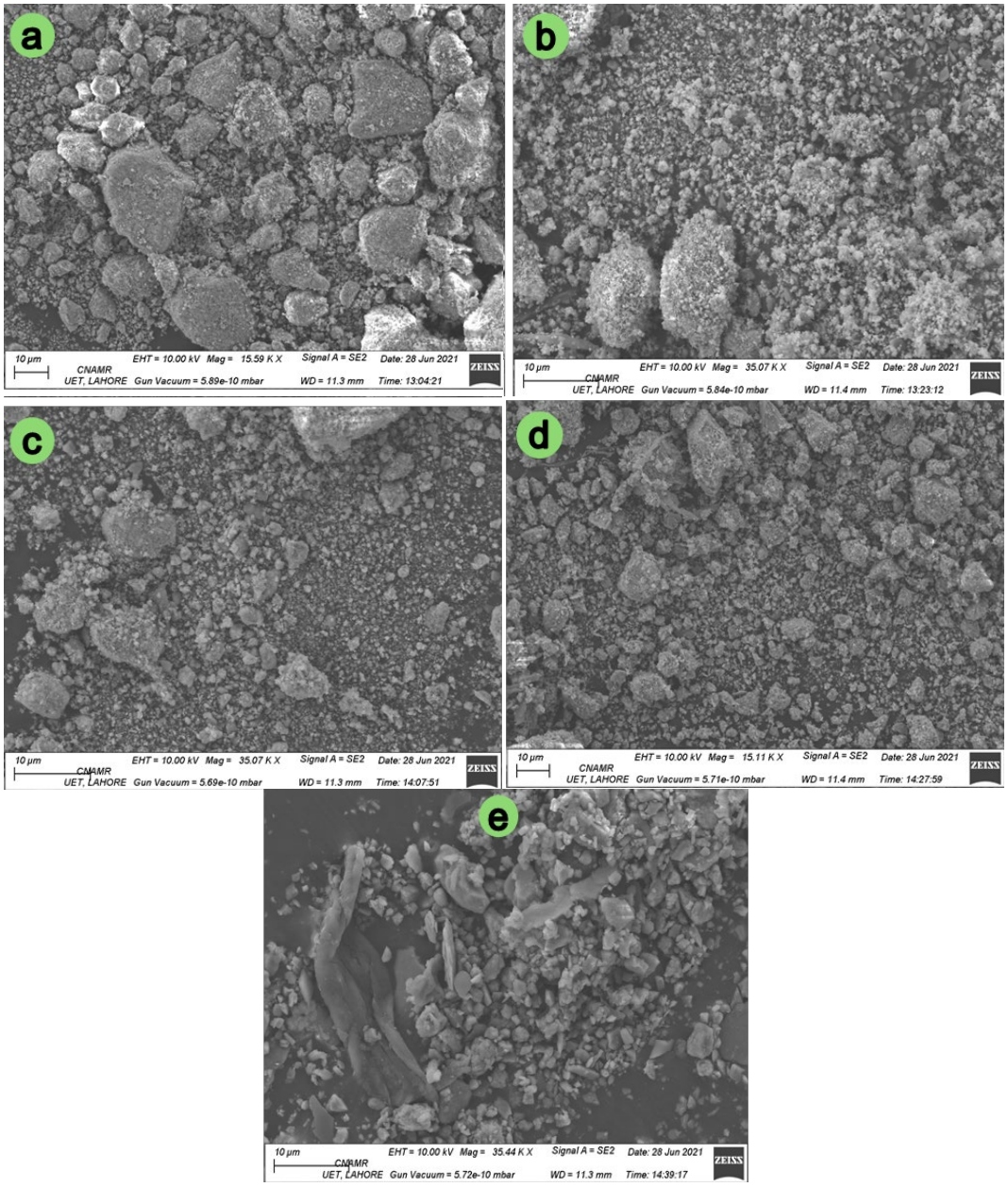


*Fig. 2. SEM images of pure (a) and Zr (0, 0.1, 0.15, 0.2, 0.25) doped $Co_3ZrxS_4$ (b-e) respectively.*

The EDX spectroscopy permits the identification of the elements in the specimen. The EDX analysis has peaks in the spectra for the real composition of the elements in the synthesized sample. This analysis may be semi-qualitative and quantitative, and elemental composition has been shown in Figs. 3 (a-e). EDX spectra for pure $CoS_2$ shows peaks for Co and S (Fig. 3a). In comparison, EDX of all samples of Zr (0, 0.1, 0.15, 0.2, 0.25) doped $Co_3ZrxS_4$ (b-e) features an extra peak of relatively modest strength, demonstrating Zr substitution (Figs. 3 (b-e). Elemental results from analysis indicate the effective synthesis of $Co_3S_4$ and $Zr.Co_3S_4$ [34].

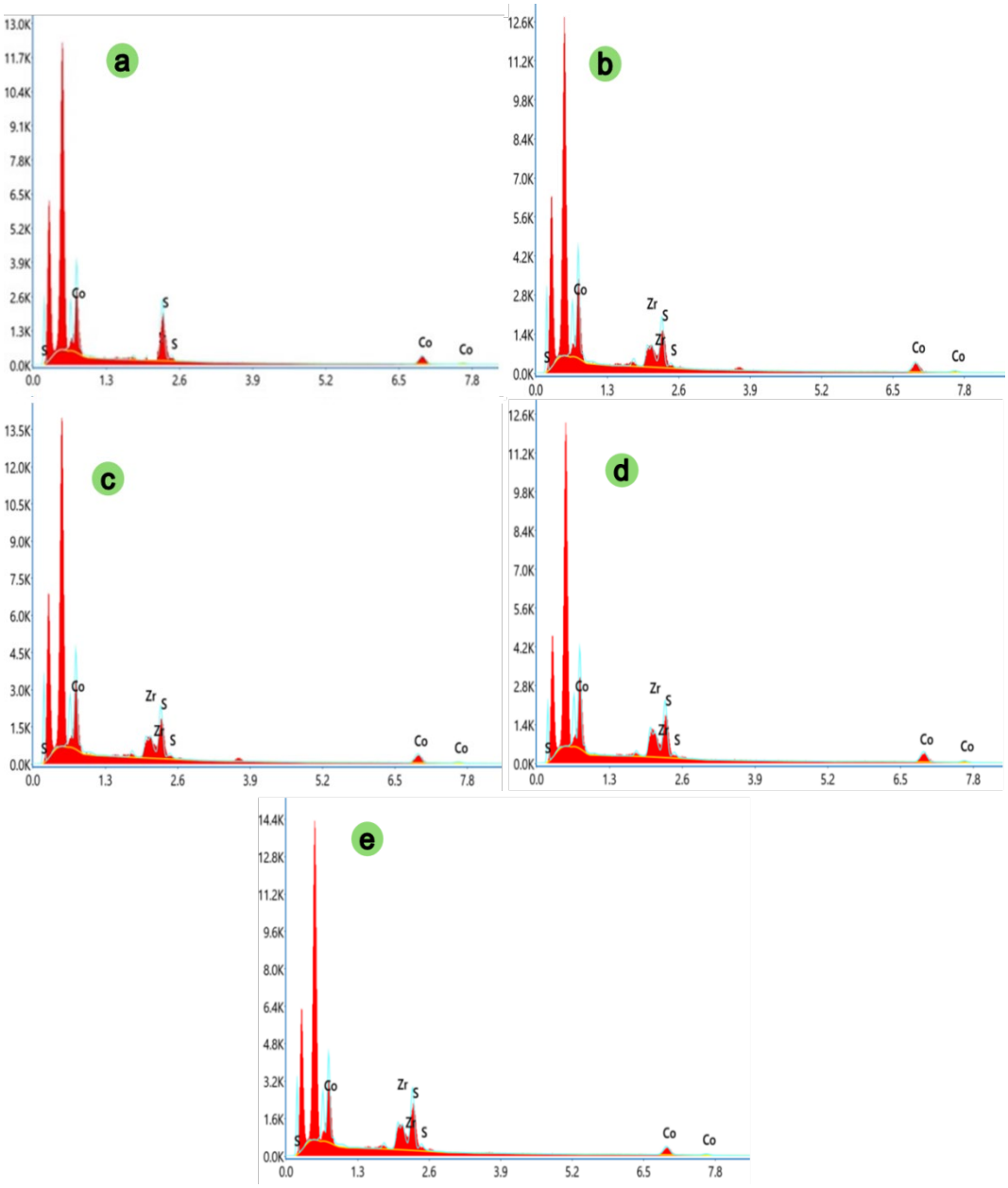


*Fig. 3. EDX images of pure (a) and Zr (0, 0.1, 0.15, 0.2, 0.25) doped $Co_3ZrxS_4$ (b-e) respectively.*

### 3.3. FTIR analysis

FTIR analysis is employed to study the chemical bonding and to identify functional groups in the material. From the results of FTIR, it is interpreted that they have shown the frequencies of the absorption in the pure and the Zr doped $Co_3S_4$ nanoparticles. The band of the spectrum below 1000cm$^{-1}$ is known as the region of the fingerprints. The bands showing up at 560, 670 and 857cm$^{-1}$ are known as the characterized bands of the Sulfides that satisfy the formulation of the $Co_3S_4$. The broader band at 1080cm$^{-1}$ shows the presence of the O-H group, which expresses the hydrous nature of the prepared sample [35]. The FTIR spectra show the same resulting graphs as shown in Fig. 4 without any fluctuation between the pure and Zr-doped $Co_3S_4$, which indicates the full incorporation of the Zr in the moderator material.

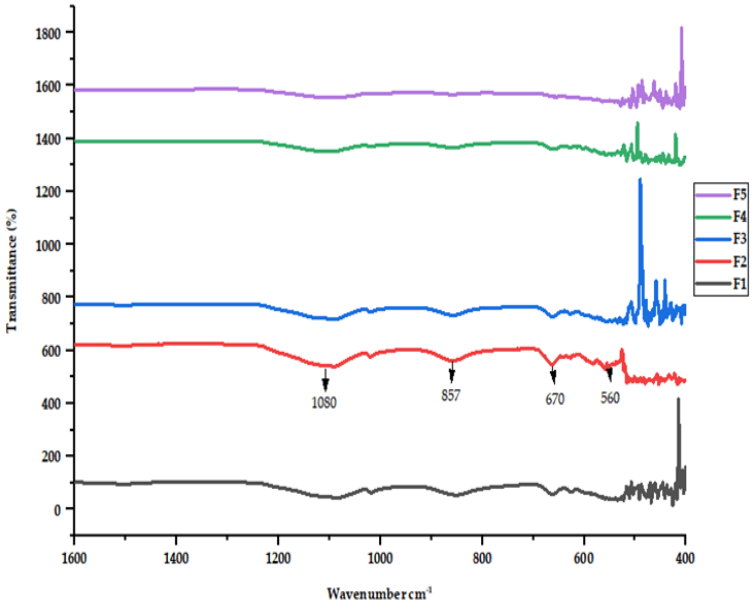


*Fig. 1. FTIR Spectra of pure and Zr (0, 0.1, 0.15, 0.2, 0.25) doped $Co_3ZrxS_4$ respectively.*

### 3.4. Raman spectroscopy

Raman spectroscopy gives detailed information about vibrational modes of material and the effect of doping on lattice. The Raman spectra of the Zr-doped cobalt Sulfide ($Co_3Zr_xS_4$) nanoparticle has been shown in Fig. 5. The region below the 1500cm$^{-1}$ in the Raman shift is detected as a fingerprint region of a substance which is specified. This region is also known as a characteristic pattern. This spectrum showed stokes region. Here the peaks of the Raman shifts determine the specified vibration modes of the cobalt Sulfide. The peak at 292cm$^{-1}$ and 475cm$^{-1}$ showed the $E_g$ value, the peak at 323cm$^{-1}$ showed the $T_g$ value, the peaks at the 393cm$^{-1}$ showed the $A_g$ value, the peak at the 517cm$^{-1}$ determine the $F_{2g}$ value and the peak at the 676cm$^{-1}$ determine the $A_{1g}$ value for the cobalt Sulfides nanoparticle [36].

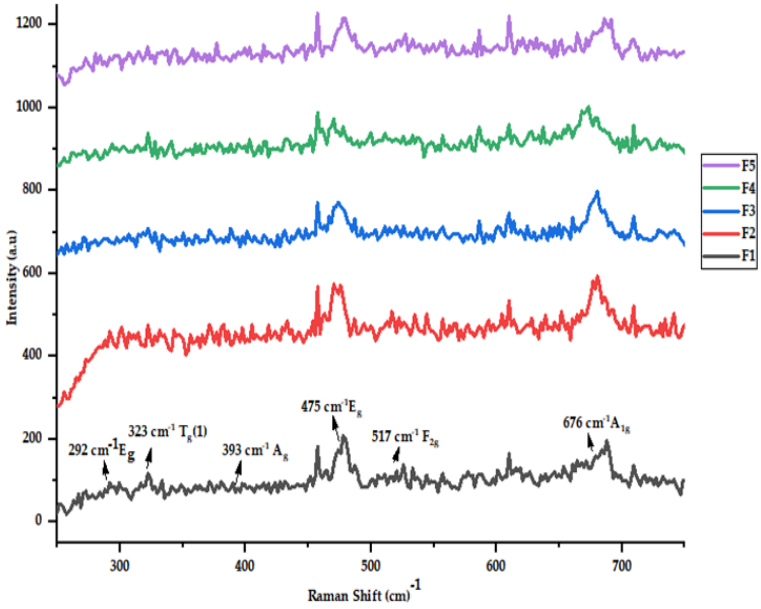


*Fig. 2. Raman spectra of pure and Zr (0, 0.1, 0.15, 0.2, 0.25) doped $Co_3ZrxS_4$ respectively.*

### 3.5. PL characterization

The technique of photoluminescence spectroscopy is commonly used to characterize the optical as well as electrical characterizations of semiconductors. The results of the PL for the pure and Zr-doped Cobalt Sulfide ($Co_3Zr_xS_4$) are shown in Fig. 6. The band gap value for the pure and Zirconium-doped cobalt sulfide ranges from 1.4 to 1.96. The results showed that Zr-doping shifted the PL spectra, increased the band gap and enhanced the efficiency of absorption of photon and recombination efficiency.

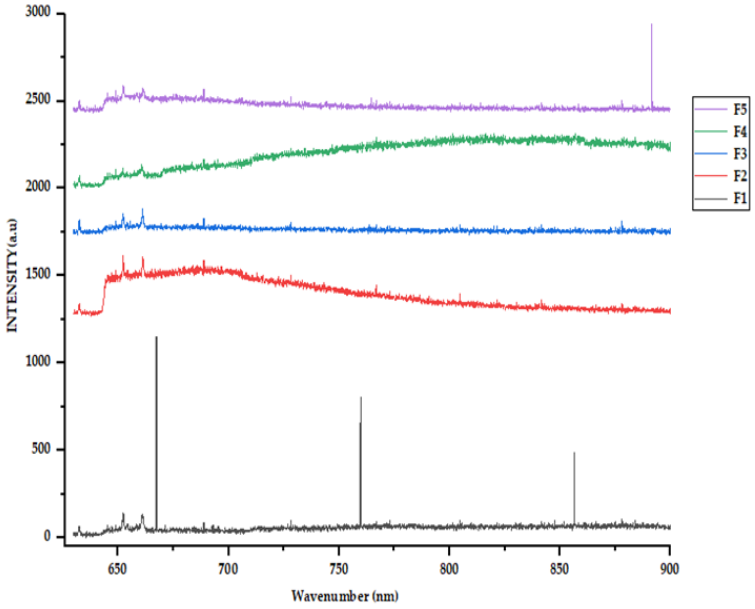


*Fig. 3. PL Spectra for pure and Zr (0.1, 0.15, 0.2, 0.25) doped $Co_3ZrxS_4$ respectively.*

### 3.6. UV-VIS spectroscopy

UV-Visible spectroscopy is employed to give valuable information about optical properties and electronic structure of pure and $Co_3S_4$ NPs. The absorbance curve for pure and Zr-doped $Co_3S_4$ with different concentrations of Zr can be observed in Fig. 7, demonstrating that the particles absorb radiation in the visible spectrum of radiations (400nm-600nm). When compared, the nanoparticles of the pure $Co_3S_4$ with the nanoparticles of the doped $Co_3Zr_xS_4$ absorb more light. A red shift is observed for $Co_9Zr_xS_4$ absorbance wavelength. The shifting of absorbance edge toward the longer wavelength verifies the Zr doping in $Co_3S_4$. Tauc's technique was employed to estimate the band-gap value ($E_g$) for pure and Zr-doped $Co_9S_4$. According to Tauc, the difference between photon energy and band gap determines the intensity of optical absorption.

Tauc's relation is expressed as:

$$(ahv)^{1/n} = A\,(hv - E_g) \tag{2}$$

Here, h is the plank's constant, A is the proportionality constant, $hv$ is the input photon energy, and *Eg* is the band gap. To obtain the band-gap value, draw a graph $(hv)^2$ between and h. The band gap for undoped $Co_3S_4$ is 2.08eV, whereas Eg values for doped samples range from 2.09 to 2.13eV.

Table 1 shows the band-gap values for each sample. The link between them depicts the relationship between Zr concentration and the energy band gap. As Zr concentration rises, the band gap also increases.

*Table 1. Band gap value of pure and doped sample.*

| Sample | Eg (eV) |
|---|---|
| F1 ( $Co_3S_4$) | 2.08 |
| F2 ($Co_3Zr_{0.1}S_4$) | 2.09 |
| F3 ($Co_3Zr_{0.15}S_4$) | 2.07 |
| F4 ($Co_3Zr_{0.2}S_4$) | 2.14 |
| F5 ($Co_3Zr_{0.25}S_4$) | 2.13 |

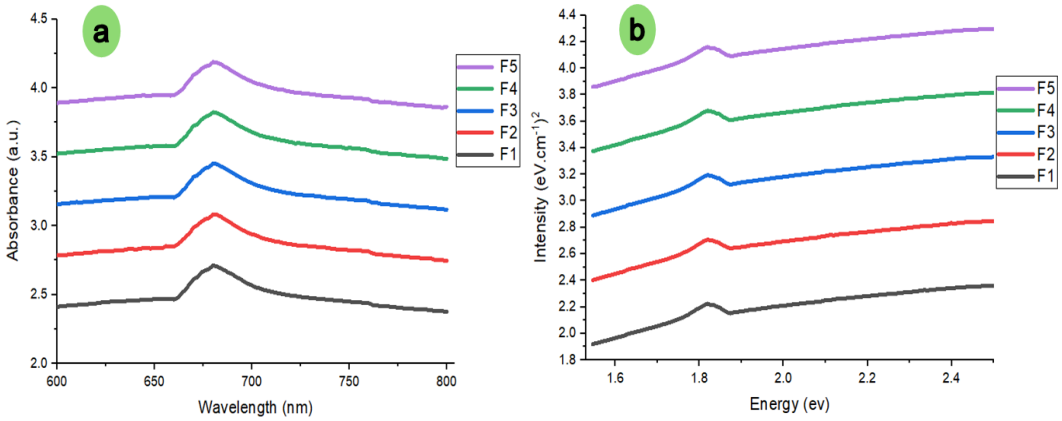


*Fig. 4. Absorption spectra (a) and Tauc plot of pure and Zr (0.1, 0.15, 0.2, 0.25) doped $Co_3ZrxS_4$ (b) respectively.*

### 3.7. Thermoelectric effect

The thermoelectric effect is used to assess the influence of Zr doping on cobalt sulfide nanoparticles' thermoelectric performance. The results of the thermoelectric effect of the synthesized sample have been shown in Fig.8. The result showed that the current value depends upon the temperature. The electrical parameters found that a slight increase in the concentration of the Zirconium would show a decline in the current value. Initially, the increase in the concentration showed a minute change in the current value, but after a unique value of the temperature, it showed a great decrease in the current value.

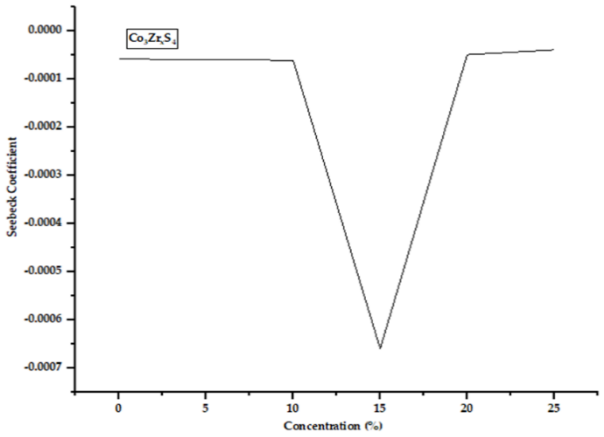


*Fig. 8. Thermoelectric behavior of pure and Zr doped $Co_3Zr_XS_4$.*

With the increase in the concentration of the zirconium, the increase in the critical temperature was reported, which produced crystal defects and can change the number of the charge carriers in the cobalt sulfide, consecutively decreasing the current value [35].

### 3.8. I-V characteristic

The current-voltage (I-V) response of pure and Zr doped $Co_3S_4$-NPs at different concentrations were examined employing the two-probe I-V approach and the corresponding results are shown in Fig. 9. The current and voltage curves of a pure sample were found to have a linear relationship. Electrical conductivity can be calculated by using the relation such as:

$$\text{Conductivity} = \alpha = \frac{L}{RA} \tag{3}$$

where L is the thickness, R is resistivity and A is area of the pallet. Table 2 showed the observed conductivity and resistivity of the samples with different Zr concentrations. The I-V curve predicts that as the Zr content rises a random change shown in the resistivity ($\rho$) and the conductivity ($\alpha$ ). Zr ions, which are replaced at Co ions sites, have an influence on the number of charge carriers and the mobility of charge carriers.

*Table 2. Study on the influence of zirconium doping on the electrical properties of $Co_3S_4$.*

| Samples | Resistivity (Ohm.m) | Conductivity $(Ohm.m)^{-1}$ |
|---|---|---|
| F1 $(Co_3S_4)$ | 3.6E-05 | 2.7E+4 |
| F2 $(Co_3Zr_{0.1}S_4)$ | 4.1E-05 | 2.4E+4 |
| F3 $(Co_3Zr_{0.15}S_4)$ | 1.3E-4 | 7.6E+4 |
| F4 $(Co_3Zr_{0.2}S_4)$ | 2.7E-05 | 3.6E+4 |
| F5 $(Co_3Zr_{0.25}S_4)$ | 1.4E-4 | 7.1 E+3 |

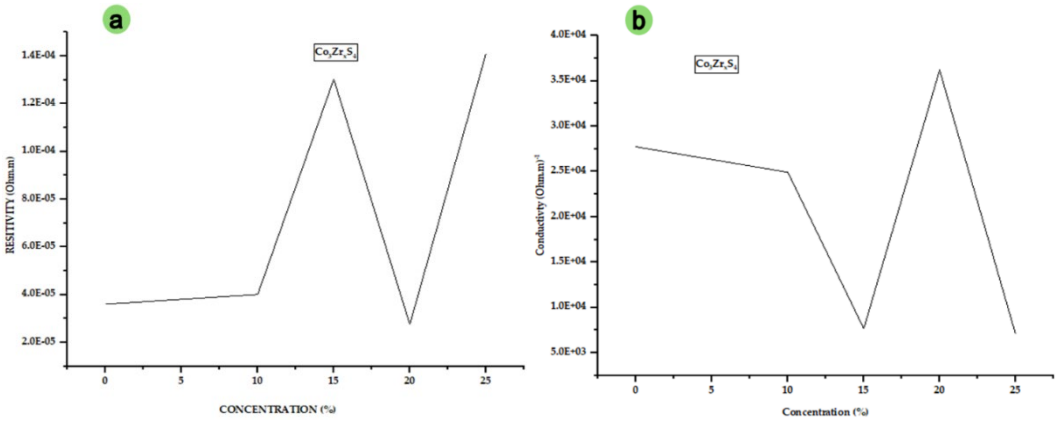


*Fig. 3. (a) Electric parameter (Resistivity) vs Zr concentration curve*
*(b) Electric parameter (Conductivity) vs Zr concentration curve.*

## 4. Conclusion

$Co_3S_4$ and Zr-doped $Co_3S_4$ (0%, 5%, 10%, 15% and 20%) NPs were synthesized via chemical co-precipitation method and then characterized. The cubic structure of $Co_3S_4$ nanoparticles, with a lattice constant of 7.9 Å and crystallite sizes ranging from 2.29 to 54.42 nm, was confirmed by XRD analysis. SEM images revealed that grain size decreased as the dopant concentration increased. Additionally, the band-gap energy rose slightly from 2.08 eV to 2.13 eV with the introduction of zirconium dopant. The material's strong optical absorbance highlights its potential suitability for photocatalytic applications. In the thermoelectric effect analysis of the prepared sample, an increase in zirconium concentration led to a rise in the critical temperature. This is attributed to the incorporation of zirconium, which creates crystal defects. These defects alter the number of charge carriers in cobalt sulfide. As a result, the current value decreases consecutively. I-V curve predicts that as the Zr content rises, a random change shown in the resistivity ($\rho$) and the conductivity ($\alpha$ ). Zr ions, which are replaced at Co ions sites, have an influence on the number of charge carriers and the mobility of charge carriers.

## References

[1] X. Wang, Wang J., Yang Y., Wu Q., Zhang C., Wang J., Xu R., Yang L. Applied Surface Science 640, 158361 (2023); https://doi.org/10.1016/j.apsusc.2023.158361

[2] K. Patil, Babar P., Bae H., Jo E., Jang J. S., Bhoite P., Kolekar S., Kim J. H. Sustainable Energy & Fuels 6(2), 474-83 (2022); https://doi.org/10.1039/D1SE01478A

[3] J. Cheng, Wang D. Chinese Journal of Catalysis;43(6):1380-98 (2022); https://doi.org/10.1016/S1872-2067(21)63987-6

[4] Z. N. Zahran, Mohamed E. A., Tsubonouchi Y., Ishizaki M., Togashi T., Kurihara M., Saito K., Yui T., Yagi M. Energy & Environmental Science 14(10), 5358-65 (2021); https://doi.org/10.1039/D1EE00509J

[5] P. M. Bodhankar, Sarawade P. B., Kumar P., Vinu A., Kulkarni A. P., Lokhande C. D., Dhawale D. S. Small 18(21), 2107572 (2022); https://doi.org/10.1002/smll.202107572

[6] Y. Lu, Li Z., Xu Y., Tang L., Xu S., Li D., Zhu J., Jiang D. Chemical Engineering Journal, 411, 128433 (2021); https://doi.org/10.1016/j.cej.2021.128433

[7] S. Ibraheem, Yasin G., Kumar A., Mushtaq M. A., Ibrahim S., Iqbal R., Tabish M., Ali S., Saad A. Applied Catalysis B: Environmental 304, 120987 (2022); https://doi.org/10.1016/j.apcatb.2021.120987

[8] A. Pandey, Yadav P., Biswal R., Fahad A., Khan B., Kumar P., Singh M. K. Ferroelectrics 618(2), 451-63 (2024); https://doi.org/10.1080/00150193.2023.2273722

[9] J. Gautam, Liu Y., Gu J., Ma Z., Zha J., Dahal B., Zhang L. N., Chishti A. N., Ni L., Diao G. Advanced Functional Materials 31(46), 2106147 (2021); https://doi.org/10.1002/adfm.202106147

[10] Z. Zheng, Yu L., Gao M., Chen X., Zhou W., Ma C., Wu L., Zhu J., Meng X., Hu J. Nature communications 11(1), 3315 (2020); https://doi.org/10.1038/s41467-020-17199-0

[11] B. Dutta, Wu Y., Chen J., Wang J., He J., Sharafeldin M., Kerns P., Jin L., Dongare A. M., Rusling J. ACS Catalysis 9(1), 456-65 (2018); https://doi.org/10.1021/acscatal.8b02904

[12] K. P. Sharma, Shin M., Awasthi G. P., Yu C. Current Applied Physics 56, 126-34 (2023); https://doi.org/10.1016/j.cap.2023.10.007

[13] B. Wang, Chen Y., Wang X., Zhang X., Hu Y., Yu B., Yang D., Zhang W. Journal of Power Sources 449, 227561 (2020); https://doi.org/10.1016/j.jpowsour.2019.227561

[14] A. Alshoaibi. Materials 16(13), 4512 (2023); https://doi.org/10.3390/ma16134512

[15] N. Maile, Shinde S., Kim D. Y., Devarayapalli K., Lee D. S. Journal of Alloys and Compounds 967, 171845 (2023); https://doi.org/10.1016/j.jallcom.2023.171845

[16] X. Zhu, Tao H., Li M. International Journal of Hydrogen Energy 45(28), 14452-60 (2020); https://doi.org/10.1016/j.ijhydene.2020.02.188

[17] J. Sharma, Gupta A., Pandey O. Ceramics International 45(11), 13671-8 (2019); https://doi.org/10.1016/j.ceramint.2019.04.061

[18] F. Zhang, Cho M., Eom T., Kang C., Lee H. Ceramics International 45(16), 20972-6 (2019); https://doi.org/10.1016/j.ceramint.2019.06.240

[19] Q. Zhang, Cao D., Ma Y., Natan A., Aurora P., Zhu H. Advanced Materials 31(44), 1901131 (2019); https://doi.org/10.1002/adma.201901131

[20] E. Sathiyaraj, Thirumaran S. Chemical Physics Letters 739, 136972 (2020); https://doi.org/10.1016/j.cplett.2019.136972

[21] D. Nam, Jang E., Kim J. Journal of Alloys and Compounds 947, 169625 (2023); https://doi.org/10.1016/j.jallcom.2023.169625

[22] T. He, Zhao W., Hu J., Deng C., Yan D., Huang S. Advanced Functional Materials 34(8), 2310256 (2024); https://doi.org/10.1002/adfm.202310256

[23] Y. Gao, Wang Y., Jiang J., Wei P., Sun, H. Small 21(11), 2411432. (2025); https://doi.org/10.1002/smll.202411432

[24] L. Wu, Jiang Y., Peng Z., Wang X., Hou C., Liu Y., Chen K. Journal of Environmental Chemical Engineering 113869 (2024); https://doi.org/10.1016/j.jece.2024.113869

[25] Z. Liu, Gao Z., Wu Q. Chemical Engineering Journal 423, 130283 (2021); https://doi.org/10.1016/j.cej.2021.130283

[26] X. Li, Liu J., Lv R., Chu Y., Lv L., Lu J., Zhang W. Chemical Engineering Journal 463, 142369 (2023); https://doi.org/10.1016/j.cej.2023.142369

[27] Y. Zhao. Journal of Materials Research echnology, 21, 546-560 (2022); https://doi.org/10.1016/j.jmrt.2022.09.032

[28] S. Zhang, Li J, Tian Y, Fang S, Li C, Yu X, Jiang Y, Yang L. Combustion and Flame 272, 113858 (2025); https://doi.org/10.1016/j.combustflame.2024.113858

[29] X. Qin, Li H., Wang K., Liu Y., Song L., Lin Y., Fan F., Li S., Ma T. Process Safety and Environmental Protection 183, 163-77 (2024); https://doi.org/10.1016/j.psep.2024.01.010

[30] T. Munir, Mahmood A., Fatima S., Sohail A., Fakhar-e-Alam M., Atif M., Rafaqat N. Journal of King Saud University-Science 35(7), 102836 (2023); https://doi.org/10.1016/j.jksus.2023.102836

[31] S. Chakraborty. Biophysical Reviews and Letters, 1 (2024); https://doi.org/10.1142/S1793048024500073

[32] J. Joshi, Kanchan D., Joshi M., Jethva H., Parikh K. Materials Research Bulletin 93, 63 (2017); https://doi.org/10.1016/j.materresbull.2017.04.013

[33] H. Sharma, Surbhi, Vinod A., Rathore M. S. Journal of Electronic Materials 53(1), 41 (2024); https://doi.org/10.1007/s11664-023-10781-4

[34] P. O. Agboola, Shakir I., Almutairi Z. A., Shar S. S. Ceramics International 48(6), 8509 (2022); https://doi.org/10.1016/j.ceramint.2021.12.061

[35] T. Munir, ur Rehman N., Mahmood A., Mahmood K., Ali A., Khan I., Sohail A., Manzoor A. Chemical Physics Letters 761, 137989 (2020); https://doi.org/10.1016/j.cplett.2020.137989

[36] D. Ma, Hu B., Wu W., Liu X., Zai J., Shu C., Tadesse Tsega T., Chen L., Qian X., Liu T. L. Nature Communications 10(1), 3367 (2019); https://doi.org/10.1038/s41467-019-11176-y